Single-cell RNA sequencing reveals functional heterogeneity and sex differences of glioma-associated brain macrophages

Natalia Ochocka[1#], Pawel Segit[1#], Kacper Adam Walentynowicz[1], Kamil Wojnicki[1], Salwador Cyranowski[1], Julian Swatler[2], Jakub Mieczkowski[1]*, Bozena Kaminska[1]*

[1] Laboratory of Molecular Neurobiology, Nencki Institute of Experimental Biology of the Polish Academy of Sciences, Warsaw, Poland

[2] Laboratory of Cytometry, Nencki Institute of Experimental Biology of the Polish Academy of Sciences, Warsaw, Poland

#Equally contributing

*Corresponding authors: b.kaminska@nencki.gov.pl; j.mieczkowski@nencki.gov.pl

Abstract

Brain resident and infiltrating innate immune cells adapt a tumor-supportive phenotype in the glioma microenvironment. Flow cytometry analysis supported by a single-cell RNA sequencing study of human gliomas indicate considerable cell type heterogeneity. It remains disputable whether microglia and infiltrating macrophages have the same or distinct roles in supporting glioma progression. Here, we performed single-cell transcriptomics analyses of CD11b+ cells sorted from murine syngeneic gliomas, indicating distinct activity of microglia, infiltrating monocytes/macrophages and CNS border-associated macrophages. Our results demonstrate a previously immeasurable scale of molecular heterogeneity in the innate immune response in gliomas. We identified genes differentially expressed in activated microglia from glioma-bearing mice of different sex, and profound overexpression of the *MHCII* genes by male microglial cells, which we also observed in bulk human glioma samples. Sex-specific gene expression in microglia in the glioma microenvironment may be relevant to sex differences in incidence and outcomes of glioblastoma patients.

Introduction

Infiltrating immune system cells represent an abundant non-malignant component of the tumor microenvironment (TME). These cells play a pivotal role in tumor progression and modulation of tumor responses to therapy[1]. A high number of macrophages within TME have been associated with a poor prognosis in many cancers because those tumor-educated cells suppress anti-tumor immunity, stimulate angiogenesis, and promote tumor invasion[2].

The central nervous system (CNS) is equipped with resident innate immune cells—microglia and CNS border-associated macrophages (BAMs)—consisting of perivascular, meningeal, and the choroid plexus macrophages. Those cells migrate to the CNS early in the prenatal life and maintain a long-lasting population. In malignant gliomas, besides activation of local microglia, circulating monocytes invade the brain from the periphery and differentiate within the tumor; therefore, microglia and infiltrating monocytes/macrophages are commonly referred to as glioma-associated macrophages (GAMs), due to the shortage of immunocytochemical markers allowing their reliable identification[3]. Transcriptome profiling of bulk CD11b+ cells isolated from human glioblastomas (GBMs) and rodent gliomas showed a mixture of protumorigenic and antitumorigenic phenotypes and did not reveal consistent markers and pathways[4–6]. Recent reports have demonstrated that GAMs consist of diverse cell populations with likely distinct roles in tumor progression[7–10]. Dissecting the TME composition and functional heterogeneity of tumor-infiltrating immune cells would extend the understanding of the glioma immune microenvironment and allow to modulate functions of distinct subpopulations for therapeutic benefits.

Sex differences in incidence, transcriptomes, and patient outcomes in the adult GBM patients have been reported, providing an explanation for GBM occurrence with a male-to-female ratio of 1.6:1[11]. The sex-specific outcome can be related to immune function because the efficacy of cancer immunotherapy was found to be sex dependent, with better outcomes in males[12]. Transcriptomic studies of male and female microglia demonstrated that in naïve mice, male microglia show enrichment of inflammation and antigen presentation-related genes, whereas female microglia have a higher neuroprotective capacity[13,14]. Until now, sex differences have been largely unexplored in animal studies on glioma immunobiology.

Here, we used single-cell transcriptomics (scRNA-seq) to decipher the composition and functions of GAMs in murine experimental gliomas growing in male and female mice. We demonstrate distinct transcriptional programs of microglia, infiltrating monocytes/macrophages, and CNS BAMs. The identified microglia and monocyte/macrophage signature markers allow for clear separation of these cells within glioma TME. We demonstrate that in the presence of glioma, microglia and

monocytes/macrophages activate similar transcriptional networks. However, the transcriptional response of monocytes/macrophages is more pronounced and associated with activation of immunosuppressive genes. A subset of macrophages expresses *Cd274* mRNA (coding for PD-L1). Moreover, we found that in males, both microglia and a substantial fraction of monocytes/macrophages from gliomas express a higher level of the *MHCII* genes, an observation that correlates with an increased number of CD4+ T cells in the male versus female TME. This work demonstrates a cell type heterogeneity and sex-specific differences of immune cells infiltrating gliomas.

Results

Single-cell RNA-seq identifies distinct subpopulations amongst CD11b+ cells from naïve and glioma-bearing brains

We employed a murine orthotopic GL261 glioma model because tumors established from GL261 cells recapitulate many characteristics of human GBMs and are frequently used to study glioma immunology, immunotherapy, and in preclinical studies[15]. To assess the heterogeneity of GAMs in GL261 gliomas, we performed scRNA-seq on CD11b+ cells sorted from naïve and tumor-bearing brains of male and female mice (two replicates per group) **(Figure 1a)**. The tumor-bearing animals were sacrificed 14 days post implantation. This time point corresponds to a pre-symptomatic stage of tumorigenesis, when tumors are confined to the striatum and restricted to a single hemisphere **(Supplementary Figure 1a-d)**. At that stage, GL261 gliomas show a substantial infiltration of peripheral monocytes/macrophages[16], and no signs of necrosis. Using flow cytometry, we sorted the CD11b+ cells of a particularly high purity (>96%) and viability (~95%) **(Supplementary Figure 1e).** Inclusion of live/dead cell discrimination during sorting did not result in further improvements of cell viability; therefore, we omitted this step in order to shorten sample preparation time.

To resolve the molecular profiles of the sorted cells, we analyzed their transcriptomes using a single-cell RNA-seq technique. After quality control and accounting for technical noise, single-cell transcriptomic profiles for 40,401 cells and 14,618 genes were considered for the analysis (see Methods for details). Unsupervised clustering of each group demonstrated a similar number of clusters between sexes. For naïve female and male CD11b+ cells, 9 and 8 clusters were obtained, respectively, and 13 clusters were identified for CD11b+ cells from tumor-bearing hemispheres, for both sexes. We visually inspected the transcriptomic diversity of computed clusters, projecting the data onto two dimensions by t-distributed stochastic neighbor embedding (t-SNE) **(Figure 1b)**. To characterize the cell identity of the obtained clusters, we applied the immune cell marker panel **(Figure 1c)**

created with the literature-based markers **(Supplementary Table 1)**[3,7,8,10,17-29]**.** The cellular identities were inferred by identifying significantly overexpressed genes in each cluster. In naïve brains, microglia (MG) comprised the vast majority of all sorted cells (91% in females, 90% in males), whereas BAMs constituted 6% of cells in both sexes **(Figure 1d)**. Additionally, besides the major microglial clusters, we identified a minor population of premature microglia (pre-MG) expressing markers of microglia (*Tmem119*, *P2ry12*) and genes characteristic for their premature state (*Csf1*, *Crybb1*, *Mcm5*, *Ifit3*)[20]. Amongst CD11b+ cells from male controls, we found a small subset of monocytes (Mo, *Ly6c2*+, *Ccr2*+), natural killer (NK, *Ncam1*+), and dendritic cells (DC, *Cd24a*+), all of which were not found in female controls.

In tumor-bearing brains, microglia were still the most abundant cell population (64% in females, 65% males), although their proportion decreased due to infiltration of monocytes/macrophages (Mo/MΦ) from the periphery, forming the 2nd main myeloid cell population of the TME (23% in females, 28% in males) **(Figure 1d)**. For both sexes, we identified 3 clusters of infiltrating Mo/MΦ that could be further characterized by an inflammatory monocyte signature—Mo (*Ly6c2*^{high}, *Ccr2*^{high}, *Tgfbi*^{low})—, an intermediate state of monocyte and macrophage signature—intMoMΦ (*Ly6c2*$^{+}$, *Ccr2*^{high}, *Tgfbi*^{high})—, and a differentiated macrophage signature—MΦ (*Ly6c2*^{low}, *Ifitm2*^{high}, *Ifitm3*^{high}, *S100a6*^{high}) (**Figure 1c**). These results demonstrate the dynamics of monocyte/macrophage phenotypic changes upon infiltration to the TME. We also identified smaller populations of NK cells, DCs, natural killer T cells (NKT), and a minor fraction of B and T cells. Although CD11b+ is generally not expressed on lymphocytes, sparse populations of those cells expressing CD11b+ (>1%) may appear after activation of the immune response[30,31]. Nevertheless, a vast majority of cells were MG, Mo/MΦ, and BAM; thus, we focused on those major cell types in further analyses.

Assessment of new and known cell type specific markers

To identify the molecular features that distinguish naïve and tumor-associated myeloid cells, we performed further analyses on preselected cell subpopulations. From all the conditions and replicates, we extracted only the cells identified as microglia, monocytes/ macrophages, and BAMs. The combined three cell subpopulations, projected on the two-dimensional space using a Uniform Manifold Approximation and Projection (UMAP) algorithm, formed three separate groups that corresponded to the previously identified cell subpopulations **(Figure 2a)**. This observation demonstrates a predominance of a biological signal over technical artifacts or batch effects. To confirm cell identities, we performed differential expression analyses between these three subpopulations of CD11b+ cells. Among the most highly upregulated genes in each group (see Methods), we found the well-known microglial genes—*Cx3cr1*, *Olfml3*, *Gpr34*, *Tmem119*, *Selplg*, *Sparc*, and *P2ry12*[18,32]—, monocyte

genes—*Ly6i*, *Ly6c2*, macrophage genes—*Ifitm3*[10]—, and BAM genes—*Apoe*, *Ms4a7*, *Mrc1*[33]. These features confirmed the identity of the distinguished cell populations **(Figure 2b)**. Microglial cell group was best characterized by the expression of *Tmem119*, *Cx3cr1*, *P2ry12*, *Gpr34*, *Olfml3*, and *Sparc* **(Figure 2c)**. Some highly expressed microglial genes were found only in a fraction of cells (e.g., the *P2ry13* gene was found in less than 75% of microglial cells); other microglial genes including *Fcrls and Cd81* were also expressed in BAMs and *Hexb,* and *Cst3* was expressed both in BAMs and monocytes/macrophages (Mo/MΦ). For Mo/MΦ, we found the specific expression of previously reported genes such as *Ifitm2*, *S100a6*, and *S100a11*[10], as well as novel genes, namely *Lgals3*, *Isg15*, *Ms4a4c*, and *Crip1* **(Figure 2d)**. *Ifitm3* was highly expressed by the Mo/MΦ population, but it has been found in a substantial fraction of microglial cells, showing its low specificity towards monocytes/macrophages within glioma TME. Interestingly, among the highly upregulated Mo/MΦ genes, we found markers characterizing discrete subpopulations of the Mo/MΦ. The high *Ly6c2* expression was found in a large cell fraction, which could be further divided into *Ly6c2*^{high}*Ccr2*^{high} monocytes (Mo) and *Ly6c2*^{high}*Tgfbi*^{high} monocyte/macrophage intermediate cells (intMoMΦ) **(Figure 2e-g)**. The remaining cells resembled differentiated tissue macrophages (MΦ because they lacked the markers of the cytotoxic monocytes *Ly6c2* and *Ccr2* and had a strong "macrophage" signature (*Ifitm2*^{high}, *S100a6*^{high}, *S100a11*^{high}). Notably, we found a population of macrophages (MΦ) expressing a high level of *Cd274* (a gene coding for PD-L1, an immune checkpoint protein), and *Ccl22*, *Ccl5*, which are chemokines important for T-cell recruitment[34,35]. Such an expression pattern suggests a putative role of those cells in mediating the immunosuppressive response. Additionally, macrophages highly and specifically expressed *Tmem123*, a gene of unknown function in microglia and macrophages, encoding a transmembrane protein Porimin that mediates cell death in Jurkat cells[36] and is expressed in mature dendritic cells[37].

We also examined the expression of genes that have been recently postulated as specific markers of infiltrating monocytes/macrophages within the TME of glioma: *Itga4*[7], *Hp*, *Emilin2*, *Sell*, and *Gda*[17] **(Figure 2d)**. The expression of *Itga4* (CD49d) was generally low and limited mostly to the MΦ subpopulation that resembles the most differentiated fraction of the infiltrating macrophages and expresses a high level of *Cd274* (PD-L1). Low *Itga4* expression in our data set might be explained by an early tumor growth stage (2 weeks after glioma cell implantation) and the high content of cytotoxic monocytes compared to macrophages. In a previous study, samples were collected at later time-points—3 weeks after implantation of GL261 cells and 5 weeks after implantation of shP53-transfected cells[7]. The expression of *Hp*, *Emilin2*, *Sell*, *Gda,* the markers suggested in a recent meta-analysis of bulk RNA-seq data sets and validation at RNA and protein levels[17], was found in the fraction of Mo (*Ly6c2*^{high}, Ccr2^{high}). In addition, we examined the expression of *Tgm2* and

Gpnmb, previously reported as the genes commonly upregulated by GAMs across different glioma animal models and in patient-derived samples in a bulk RNA-seq meta-analysis[3] **(Figure 2h)**. Surprisingly, their expression was limited to the small fraction of Mo/MΦ, demonstrating that bulk RNA-seq results may be biased by genes expressed at a high level by a small subset of cells.

The third most abundant cell population in our data set were BAMs, marked by highly expressed *Apoe* and *Ms4a7* genes that were recently proposed as universal markers of macrophages residing at the CNS borders[33]. *Apoe* and *Ms4a7* were also expressed by Mo/MΦ; however, we found other highly expressed BAM genes (*Mrc1*, *Dab2*, *F13a1*, *Mgl2*, and *Pf4*) to be better for identifying the BAM population **(Figure 2i)**. Summarizing, we validated the expression of known markers at the single-cell level and obtained a good agreement of selected microglia and BAM markers in our data set with literature data. In contrast, Mo/MΦ showed substantial heterogeneity that is likely related to their differentiation state. We identified genes characterizing the specific monocyte/macrophage subpopulations.

Distinct gene expression profiles of glioma-associated microglia and monocytes/macrophages

Distribution of cells according to the conditions (naive vs tumor) revealed separation of functional subgroups of microglia. This separation was further supported by the unsupervised clustering that led to clusters either highly enriched in the cells from naïve brains representing *homeostatic microglia* (Hom-MG) or clusters dominated by cells originated from the tumor-bearing hemispheres representing *glioma-activated microglia* (Act-MG) **(Figure 3a, Supplementary Figure 3)**. This result demonstrates activation of microglia within the TME. Invading monocytes and macrophages displayed glioma-induced gene expression profiles. In contrast to microglia, we did not find any indication of the glioma-induced activation in BAMs because the cells from naïve and tumor-bearing brains distributed evenly and did not show any clusters of cells originating from tumor-bearing hemispheres (**Figure 3a**).

Using microglia and Mo/MΦ scores (defined as an average of expression levels of genes specific to and highly expressed in a given population) **(Figure 3b),** we examined whether the glioma microenvironment alters expression profiles of microglia and macrophage "signature" genes (see for details **Supplementary Table 1**). We noticed a shift towards the lower "microglia signature" score in MG from the tumor-bearing brains compared to MG from the naïve brains **(Figure 3c)**. Still, the "microglia signature" in MG from the tumor was strong and distinguishable from Mo/MΦ, allowing for clear separation of the two cell populations **(Figure 3c)**. Similarly, the "macrophage signature" score was high and distinctive for the

Mo/MΦ population. Additionally, we performed a hierarchical clustering of cells according to the expression of reported microglia and macrophage markers, resulting in clear separation of microglia and Mo/MΦ **(Figure 3d)**. This observation indicated that cell identity is retained even under the strong influence of the glioma microenvironment.

Previous reports demonstrated that microglia occupy predominantly the tumor periphery, whereas infiltrating monocytes/macrophages are found mostly within the tumor core[9,38] Using double immunostaining, we demonstrate that microglia (Tmem119+, Iba1+) adopt an amoeboid morphology in the tumor proximity and localize abundantly at the tumor edge, whereas macrophages (Tmem119-, Iba1+) are observed mostly within the tumor mass for both male and female animals **(Figure 3e, f)**.

Altogether, we show that microglia undergo glioma-induced activation reflected by upregulation of a number of genes related to cytokine signaling and extracellular matrix degradation. This activation was associated with the slight downregulation in the expression of "microglia signature" genes. Both microglia and monocytes/macrophages retain their cell identity within the TME, and the differential expression of microglia and macrophage-specific genes allows for a clear distinction between these cells.

Transcriptional networks induced in microglia by glioma are present and more pronounced in infiltrating monocytes/macrophages

The results presented above demonstrate that microglia and monocytes/macrophages have distinct gene expression profiles. Additionally, we sought to determine whether microglia and infiltrating monocytes/macrophages have common or distinct roles in supporting glioma growth. To answer this question, we examined whether MG and Mo/MΦ activate common or distinct transcriptional networks. We performed this differential expression analysis in two steps. Firstly, we extracted genes highly upregulated in microglial cells from glioma-bearing brains (significantly upregulated genes in Act-MG compared to Hom-MG) **(Figure 4a)**. Subsequently, we performed the same analysis for Act-MG and Mo/MΦ cells **(Figure 4b**). This work allowed us to find genes either common or specific for each subpopulation **(Figure 4c,d)**. We found that the majority of genes upregulated in the Act-MG are also expressed by Mo/MΦ, and their expression is usually higher in Mo/MΦ than Act-MG **(Figure 4c)**. Among commonly induced genes, we found *Ifitm3* and a group of genes encoding MHCII proteins; *Ifitm3* has been reported as a gene, the expression of which demarcates macrophages from microglia[10]. We found that *Ifitm3* was indeed highly expressed in monocytes/macrophages; however, its expression was also induced in glioma-activated microglia, although at the lower level **(Figure 4c, d)**. Besides commonly upregulated genes, we also found population-specific expression patterns. Act-MG showed a high expression of *Ccl3*, *Ccl4*, and *Ccl12* (the

chemokine-encoding genes), whereas their expression was lower in Mo/MΦ. In contrast, Mo/MΦ were characterized by the high expression of *Ifitm2* and *Ccl5* genes **(Figure 4c)**.

Next, we performed a Gene Ontology (GO) analysis of biological processes on the two sets of genes—genes significantly upregulated in Act-MG compared to Hom-MG **(Figure 4e)** and genes significantly upregulated in Mo/MΦ compared to the Act-MG **(Figure 4f)**. We found that the glioma-induced expression in MG was specifically enriched in genes related to "cytoplasmic translation" that encode ribosomal proteins, whereas in Mo/MΦ we found specific enrichment in genes related to "drug metabolic process" and "purine monophosphate metabolic process". All other terms were directly related to the immune function and were largely shared between the genes up-regulated in MG and Mo/MΦ. Both populations showed induction of genes related to "response to bacterium" and "response to interferon-gamma"; however, those terms encompassed the broader number of genes for Mo/MΦ. In addition, Mo/MΦ demonstrated the more pronounced activation of the interferon-related genes because we also identified enrichment of "response to interferon-beta" genes. The genes related to the term "antigen processing and presentation" appeared only in Act-MG; however, the majority of genes contained within this term code for the MHCII protein complex, and are also upregulated in Mo/MΦ.

There are some shared genes that are expressed at a high level in Mo/MΦ compared to their expression levels in Act-MG. The expression of *Cd52, Stat1, Isg15*, *and Usp18* is mainly upregulated in subpopulations of Mo/MΦ. Proteins encoded by those genes are involved in important immune processes: Cd52 mediates costimulatory signals for T-cell activation and proliferation[39], Stat1 is a mediator of interferon signaling, Isg15 stabilizes STAT1 preventing premature termination of an inflammatory response[40], and Usp18 maintains microglia in a quiescent state via negative regulation of *Stat1* expression and termination of interferon-induced genes[41] **(Figure 4g)**. Such expression patterns may indicate that both microglia and monocytes/macrophages successfully initiate some elements of the immune response; however, such activation is more prominent in monocytes/macrophages. In addition, among genes that were highly expressed in Mo/MΦ, we found *Il1b* coding for an inflammatory cytokine IL-1β along with *Il1rn* and *Il18b* coding for the inhibitors of pro-inflammatory cytokines. These data, together with the high expression of *Cd274* coding for PD-L1 in Mo/MΦ, suggest the specific activation of immunosuppressive pathways in monocytes/macrophages (**Figure 4h**).

Sex-related differences in microglial expression of *MHCII* genes and infiltration of CD4+ T cells in gliomas

Sex is an important prognostic marker in GBM patients influencing incidence and disease outcomes[11,42]. Differences between male and female microglia in naïve mice have been reported[13,14]. Thus, we sought to determine whether there are sex-related differences in the expression of genes in myeloid populations within the TME. Importantly, the unsupervised cell clustering showed that microglia from glioma-bearing brains, but not from naïve brains, segregate into clusters that are enriched either in cells originating from female or male brains **(Figure 5a, Supplementary Figure 4a)**. Similarly, we noticed the sex-driven cell clustering within the intMoMΦ subpopulation of monocytes/macrophages, pointing to differences in immune cell activation in male and female mice **(Figure 5a, Supplementary Figure 4b)**.

The search for differentially expressed genes revealed that in Act-MG from males, the most highly upregulated genes are the genes coding for MHCII (*H2-Ab1*, *H2-Eb1*, *H2-Aa*) and *Cd74*—encoding an invariant MHCII chain that regulates folding and trafficking of the MHCII proteins **(Figure 5b)**. The increased expression of the *MHCII* genes and *Cd74* colocalizes with the male-dominated cell clusters found in the Act-MG, but also in the intMoMΦ population **(Figure 5c)**. This co-localization was not observed in naïve mice (**Figure 5d**). Accordingly, the cells with the high expression of *MHCII* and *Cd74* genes were enriched in Act-MG and intMoMΦ in males. This enrichment was not observed in other subpopulations: Hom-MG, Mo, MΦ, and BAMs **(Figure 5d**). Moreover, intMoMΦ in males upregulated *Mif,* encoding a macrophage migration inhibitory factor, an inflammatory cytokine that binds with a high affinity to CD74, inducing a pro-inflammatory response and CCL2-mediated macrophage migration and cell proliferation[43,44]. The increased expression of *Mif* in cells with the high expression of *MHCII* genes was restricted to the intMoMΦ subpopulation and not detected in the Act-MG **(Figure 5e).** This observation suggests that although high expression of *MHCII* genes is found in males in both glioma-activated microglia and a substantial fraction of infiltrating monocytes/macrophages, it may exert different effects in those two cell populations. The flow cytometry analysis run on the same cell pool, which was used to perform with the scRNA-seq, showed an elevated number of CD4+ T-cells in tumor-bearing hemispheres from males compared to females. **(Figure 5f)**. We explored the human glioma expression data from The Cancer Genome Atlas (TCGA) to determine whether sex has an impact on the expression of *MHCII* and *CD74* genes. High-grade glioma samples were not discriminated by the expression levels of the selected *MHCII* and *CD74* genes (data not shown), irrespective of *IDH1* mutation status or macrophage content as estimated with the xCell, a gene signature-based method inferring 64 immune and stromal cell types[45]. However, the expression of *MHCII* and *CD74* genes stratified glioma WHO grade II patients into the female-enriched *MHCII*^{low} group and the male-enriched *MHCII*^{high} group **(Figure 5g)**. This observation shows that the differential regulation of genes coding for MHCII complex between sexes is not limited to a mouse glioma model, and those

differences could be of clinical relevance. Altogether, we demonstrate that transcriptional responses of microglia to glioma varies between sexes, and microglia from tumor-bearing brains in males exhibit more prominent antigen presentation processes compared to their female counterparts.

Discussion

In the present study, we have used cell sorting and single-cell RNA sequencing to dissect the cellular and functional heterogeneity of GAMs. Although it has been known that human glioblastomas, the most malignant primary brain tumors, are infiltrated with resident microglia and bone marrow (BM) derived-macrophages, cell identities and functions of a specific subpopulations could not be inferred from bulk RNA-seq data. GAMs support glioma progression by augmenting tumor invasion, angiogenesis, and inducing immunosuppression[2], therefore, identifying specific roles of various cells is critical for a cell-specific intervention. Transcriptomic analyses of bulk CD11b+ infiltrates from human GBMs and murine gliomas showed a mixture of profiles characteristic for both pro- and antitumor phenotypes[4,46]. A commonly used strategy for cell separation based on CD45 expression has been criticized due to upregulation of CD45 by microglial cells under pathological conditions[47]. Studies with genetic lineage tracing showed that BM-derived macrophages accumulate in GL261 gliomas and transgenic RCAS-PDGF-B-HA gliomas, and transcriptional networks associated with tumor-mediated education in brain-resident microglia and recruited BM-macrophages are distinct[7,38]. Cell type-specific chromatin landscapes established before tumor initiation contributed to transcriptional differences. A study using high-resolution open-skull 2-photon microscopy demonstrated both the presence of microglia and BM-derived macrophages with distinct migratory propensities infiltrating gliomas[48]. Anti-vascular endothelial growth factor A blockade reduced GAM infiltration, particularly BM-derived macrophages[48].

The single-cell resolution achieved in this study clearly demonstrated cellular and functional heterogeneity of GAMs in experimental murine gliomas. We show that at the pre-symptomatic stage of glioma growth, microglia are the main myeloid population within the glioma TME, whereas monocytes/macrophages constitute a quarter and BAMs less than 4% of CD11b+ cells. Using immunofluorescence and double staining for Tmem119 and Iba1, we demonstrated that cell distribution within the tumor is not uniform because, in the tumor core, we found prevailing monocytes/macrophages (Tmem119-, Iba1+ cells), whereas microglia (Tmem119+, Iba1+ cells) occupied the tumor edge and periphery. This result is in agreement with previous reports on mouse experimental gliomas and a single-cell RNA-seq study on matched patient-derived samples from tumor core and periphery[9,38].

351 Microglia and macrophage transcription regulatory networks adapt to changing
352 environments[49,50]. ScRNA-seq studies on human GBMs suggested that microglia and
353 monocytes/macrophages diminish their signature of origin, impeding clear separation and
354 forming a phenotypic continuum[8,10]. We performed a detailed analysis of "microglia"
355 and "macrophage" transcriptional signatures, and the unsupervised cell clustering yielded
356 three cell clusters representing microglia, monocytes/macrophages, and CNS BAMs. A cell
357 identity was inferred based on the most highly differentially expressed genes. We discovered
358 that the "microglia signature" is indeed lower in microglial cells within the glioma TME, but the
359 expression of the signature genes is still high and distinguishable from
360 monocytes/macrophages. These observations demonstrate that cell identity is retained even
361 after cell polarization in the presence of a tumor.
362 The expression of cell identity genes does not imply functional divergence. We
363 demonstrate that glioma induces activation of similar transcriptional networks in microglia
364 and monocytes/macrophages; however, the effect is stronger in the latter cell types, likely
365 due to their prevalent localization within the tumor core, in contrast to microglia occupying
366 peripheral tumor regions[9,38]. At the same time, monocytes/macrophages specifically express
367 numerous genes related to immunosuppression BAMs and do not change their
368 transcriptional profiles in the presence of glioma.
369 Moreover, Act-MG shows high expression of *Ccl3*, *Ccl4*, and *Ccl12* (chemokine-
370 encoding genes), whereas their expression is low in Mo/MΦ. Hence, microglia respond first
371 to glioma and instigate immune cell infiltration and trafficking to the tumor site. Ccl3 and
372 Ccl12 are chemokines attracting monocytes, eosinophils, and lymphocytes, respectively.
373 Ccl12 shares the same Ccr2 receptor as two other chemokines—Ccl2 and Ccl7—in mice[51].
374 Intriguingly, infiltrating monocytes/macrophages do not form a uniform cell population,
375 and based on the cell expression profiles we distinguished cytotoxic monocytes
376 (*Ly6c2*^{high}*Ccr2*^{high}), intermediate state of monocytes-macrophages (*Ly6c2*^{high}*Tgfbi*^{high}), and
377 differentiated macrophages (*Ifitm2*^{high}, *S100a6*^{high}, *S100a11*^{high}) expressing a high level of the
378 PD-L1 encoding gene (*Cd274*). These observations suggest that monocytes arrive as anti-
379 tumor cells and upon infiltration into the TME, undergo tumor-induced phenotypic
380 differentiation. We found only a partial overlap with the recently proposed macrophage-
381 specific markers in gliomas[3,7,17], but the proportion of monocyte/macrophage subpopulations
382 may depend on the particular tumor stage. The discovered subpopulation of Mo/MΦ
383 expressing an inflammatory *Il1b*, along with *Il1rn* and *Il18b*, coding for the inhibitors of pro-
384 inflammatory cytokines, as well as *Cd274* (an immune checkpoint inhibitor), is interesting for
385 its clinical relevance, suggesting that pro-invasive and immunoregulatory functions are split
386 between microglia and macrophages, respectively.

The second important finding refers to sex-dependent differences in microglial responses to glioma. Bulk CD11b+ RNA-seq showed that in naïve mice, male microglia express a higher level of *MHCI* and *MHCII* genes and are more reactive to ATP stimulation[13]. This proposal has not been confirmed in the current scRNA-seq study, likely due to technical differences in cell sorting (CD11b+ beads versus flow cytometry) and sequencing methods. Contrastingly, within the tumor-bearing hemispheres, male microglia and intMoMΦ expressed a higher level of genes coding for MHCII components and Cd74, a level of expression that was not found for other cell types. Hence, upon glioma-induced activation, microglia and intMoMΦ in males have higher antigen-presenting capacity than their female counterparts. This increase was associated with the higher infiltration of CD4+ T cells to the glioma TME. CD4+ and perivascular Foxp3+ tumor-infiltrating T lymphocytes are associated with tumor angiogenesis and tumor progression in glioma patients[52], and their higher ratio over CD8+ cells correlates with unfavorable prognosis in GBM patients[53]. The analysis of human glioma TCGA datasets demonstrated sex-related differences in *MHCII* complex and *CD74* genes in WHO grade II gliomas, where anti-tumor immunity operates and may influence outcomes. Such differences were not detected in GBMs, irrespective of *IDH* mutation status and macrophage content in the TME. This result could be due to the highly immunosuppressed TME in human GBMs.

Although women have an increased susceptibility to autoimmune diseases, men have a higher risk of death for a majority of malignant cancers[54]. Despite the source of sex differences in cancer incidence and survival rate remaining unknown, anti-tumor immunity is an obvious candidate. In the immune checkpoint inhibitor therapy of various cancers, males presented better therapeutic outcome[12]. Estrogens mitigate inflammatory responses in microglia[55], and female microglia have a higher neuroprotective capability[56,57].

In sum, glioma attracts and polarizes microglia and monocytes that invade the brain from the periphery. Whereas invading monocytes express some inflammation markers, they differentiate into immunosuppressive macrophages within the tumor. Those cells retain their cell-identity signatures, occupy different tumor niches, and present a distinct degree of glioma-induced activation and specific functions. Interestingly, we found the stronger upregulation of genes of the MCHII complex in microglia and more abundant CD4+ infiltration in gliomas in males than females. Further studies on glioma immunopathology should explore this issue, ensure correct representation of both sexes and avoid extending findings from single-sex studies to the general population.

Methods

Animals

10-week-old male and female C57BL/6 mice were purchased from the Medical University of Bialystok, Poland. Animals were kept in individually ventilated cages, with free access to food and water, under a 12h/12h day and night cycle. All experimental procedures on animals were approved by the First Local Ethics Committee for Animal Experimentation in Warsaw (approval no 563/2018 and 764/2018).

Implantation of GL261 luc+/tdT+ glioma cells

Mice (12-week-old) were kept under deep anesthesia with 2% isoflurane during surgery. Using a stereotactic apparatus, a single-cell suspension of GL261 luc+tdT+ cells (80 000 cells in 1 µL of DMEM, Dulbecco modified essential medium) was implanted into the right striatum (+1 mm AP, -1.5 mm ML, -3 mm DV) at the rate of 0.25 µL per minute. To confirm the presence of the tumor, two weeks after implantation, animals received an intraperitoneal injection of 150 µg luciferin/kg body weight 10 min prior to imaging with the Xtreme *in vivo* bioluminescence imaging system [Bruker, Germany]. The images were acquired at medium binning with an exposure time of 2 min. X-ray images were acquired at the same mice position with the Xtreme equipment. The signal intensity of the region of interest (ROI) was computed using the provided software.

Tissue dissociation

Two weeks after tumor implantation, mice with gliomas and naïve animals (controls) were perfused transcardially with cold phosphate-buffered saline (PBS) to clear away blood cells from the brain. Further processing was performed on the pooled tissue from 2 animals per replicate. The tumor-bearing hemispheres and corresponding hemispheres from naïve animals were dissociated enzymatically to obtain a single-cell suspension with a Neural Tissue Dissociation Kit [Miltenyi Biotec] and gentleMACS Octo Dissociator [Miltenyi Biotec] according to the manufacturer's protocol. Next, the enzymatic reaction was stopped by the addition of Hank's Balanced Salt Solution (HBSS) with calcium and magnesium [Gibco, Germany]. The resulting cell suspension was filtered through a 70 µm and 40 µm strainer and centrifuged at 300 x g, 4 ºC for 10 min. Next, myelin was removed by centrifugation on 22% Percoll gradient. Briefly, cells were suspended in 25 mL Percoll solution (18.9 mL gradient buffer containing 5.65 mM $NaH_2PO_4H_2O$, 20 mM $Na_2HPO_42(H_2O)$, 135 mM NaCl, 5 mM KCl, 10 mM glucose, 7.4 pH; 5.5 mL Percoll [GE Healthcare, Germany]; 0.6 mL 1.5 M NaCl), overlayered with 5 mL PBS and centrifuged for 20 min at 950 g and 4 ºC, without acceleration and brakes. Next, cells were collected, washed with Stain Buffer (FBS) [#554656, BD Pharmingen], quantified using an EVE™ Automatic Cell Counter [NanoEnTek Inc., USA], and split for CD11b+ cell sorting and cytometric analysis.

Flow Cytometry

Samples were constantly handled on ice or at 4 °C avoiding direct light exposure. First, samples were incubated with LiveDead Fixable Violet Dead Cell Stain [1:1000, L34955, ThermoFisher] in PBS for 10 min to exclude dead cells. Next, samples were incubated for 10 min with rat anti-mouse CD16/CD32 Fc Block™ [1:250, #553141, BD Pharmingen] in Stain Buffer [#554656, BD Pharmingen] to reduce unspecific antibody binding. Then, cell suspensions were split and incubated for 30 min with two monoclonal antibody cocktails referred to as myeloid and lymphoid panels. The myeloid panel consisted of: CD45 PE-Cy7 [30-F11, BD Pharmingen], CD11b AF700 [M1/70, BD Pharmingen], CD49d FITC [R1-2, BioLegend], Ly6C PerCP-Cy5.5 [AL-21, BD Pharmingen], Ly6G APC [1A8, BD Pharmingen]. Lymphoid panel consisted: CD3 FITC [REA641, Miltenyi Biotec], CD4 VioGreen [REA604, Miltenyi Biotec), α-NK-1.1 APC [PK136, Miltenyi Biotec], CD11b PE [M1/70, BD Pharmingen]. Antibodies were titrated prior to staining to establish the amount yielding the best stain index. Samples were acquired using a BD LSR Fortessa Analyzer cytometer. Data were analyzed with FlowJo software (v. 10.5.3, FlowJo LLC, BD). Gates were set based on FMO (fluorescence minus one) controls and back-gating analysis. Percentages on cytograms were given as the percentage of a parental gate (myeloid & lymphoid panels) or the percentage of all alive cells (CD4 in a lymphoid panel). Flow cytometry experiments were performed at the Laboratory of Cytometry, Nencki Institute of Experimental Biology, Polish Academy of Sciences.

CD11b+ cell FACS sorting

Cells were suspended in Stain Buffer [#554656, BD Pharmingen] in a density of 1 mln cells per 100 µL. For assessment of cell viability during sort, cells were stained with LiveDead Fixable Violet Dead Cell Stain [L34955, ThermoFisher] in PBS for 10 min, and then rat anti-mouse CD16/CD32 Fc Block™ [1:250, #553141, BD Pharmingen] for 10 min, and CD11b+ Rat Anti-Mouse FITC [1:800, M1/70, BD Pharmingen] for another 20 min at 4°C. Cells sorted for single cell analysis were stained with CD11b+ Rat Anti-Mouse AF700 [M1/70, BD Pharmingen]. Following staining, cells were washed with Stain Buffer and sorted into 20% FBS in PBS.

Single-cell RNA sequencing

Directly after sorting, cell quantity and viability of CD11b+ cells were measured, and a cell suspension volume equivalent to 5000 target cells was used for further processing. Preparation of gel beads in emulsion and libraries were performed with Chromium Controller and Single-Cell Gene Expression v2 Chemistry [10x Genomics] according to the Chromium Single-Cell 3' Reagent Kits v2 User Guide provided by the manufacturer. Libraries' quality and quantity were verified with a High-Sensitivity DNA Kit [Agilent Technologies, USA] on a

2100 Bioanalyzer [Agilent Technologies, USA]. Next, sequencing was run in the rapid run flow cell and paired-end sequenced (read 1 – 26 bp, read 2 – 100 bp) on a HiSeq 1500 (Illumina, San Diego, CA 92122 USA).

Single-cell RNA-seq data preprocessing and normalization

Sequencing results were mapped to a mouse genome GRCm38 (mm10) acquired from the 10x Genomics website and quantified using a CellRanger v.3.0.1[58,59] [https://support.10xgenomics.com/single-cell-gene-expression/software/pipelines/latest/installation]. The total number of cells identified by the CellRanger was 41,059 (details in Supplementary Table 2). The median number of detected genes per cell was 1,059, and the median unique molecular identifiers (UMIs) per cell was 2,178. Data analysis was performed in R using Seurat v3[59,60]. Unless otherwise specified in the description, all other quantitative parameters were fixed to default values. To filter out possible empty droplets, low-quality cells, and possible multiplets, cells with less than 200 or more than 3,000 transcripts were excluded from the analysis. Additionally, cells of poor quality, recognized as cells with >5% of their transcripts coming from mitochondrial genes, were excluded from the downstream analysis. After applying these filters, 40,401 cells were present in the data set. Gene expression measurements for each cell were normalized by the total number of transcripts in the cell, multiplied by a default scale factor, and the normalized values were log-transformed ("LogNormalize" method). Following a Seurat workflow, for each replicate the 2,000 most highly variable genes were identified using variance stabilizing transformation ("vst"). To facilitate identification of cell types these gene sets were expanded by adding genes described as having important roles in immune cells (see Supplementary Table 3) and genes involved in cell cycle regulation[61]. This extension did not influence our conclusions.

Identification of myeloid cells

Having two biological replicates for each sex and condition (female control, female tumor, male control, male tumor), data from corresponding samples were integrated using a Seurat v3 approach[59]. First, 2000 integration anchors (i.e., cells that are mutual nearest neighbors between replicates) were found. These anchors were then used as input to the data sets integration procedure. Integrated data were scaled, and unwanted sources of variation, namely total number of counts per cell, percentage of transcripts coming from mitochondrial genes per cell, and cell cycle effect were regressed out, as described in a corresponding vignette [https://satijalab.org/seurat/v3.0/cell_cycle_vignette.html]. Data dimensionality reduction was performed using a principal component analysis (PCA), and the first 30 principal components were used in the downstream analyses. For each condition separately,

the expression profiles were then clustered using an unsupervised, graph-based approach with the resolution parameter set to 0.3. Clustering results were visualized using two-dimensional t-Distributed Stochastic Neighbor Embedding (t-SNE)[62]. Based on expression of the reported/canonical markers, the clusters dominated by myeloid cells in four conditions were identified and further analyzed.

Comparative analysis

The comparative analysis was based on the raw counts but limited to the previously selected profiles and genes (see above). For such a data set, a new set of the 2,000 most highly variable genes was identified using variance stabilizing transformation ("vst"), and this set was further expanded by adding the genes involved in cell cycle regulation. Computation of expression estimations, regression of the unwanted variation, and data dimensionality reduction were performed as described above. Next, the expression profiles were clustered using the same approach as above, but with a resolution parameter set to 0.6. After clustering, data were visualized using two-dimensional Uniform Manifold Approximation and Projection (UMAP)[63]. Based on expression of reported/canonical markers of myeloid cells, clusters with cells of interest (microglia, macrophages, and BAMs) were identified. Further analysis of the microglia cluster revealed that some sub-clusters cells originated in a significant majority from tumor samples. In contrast, there were no sub-clusters so strongly dominated by cells originated from control samples. Based on that observation, two subsets of microglial cells with distinct transcriptional profiles were identified: homeostatic microglia (Hom-MG) and activated microglia (Act-MG).

Differentially upregulated genes (signature genes) were found for each of the identity classes of interest. Significantly upregulated genes between compared groups were found using a Wilcoxon Rank Sum test implemented in Seurat v3 (min.pct = 0.25, only.pos = TRUE). These genes were subsequently used for the functional analysis and characterization of the identified clusters. Gene Ontology analysis was performed using the clusterProfiler package[64].

Analysis of TCGA data

The normalized expression values for low- and high-grade gliomas were downloaded from The Cancer Genome Atlas (TCGA) website (RNASeqV2 set available on 07/05/19). Sample annotations and *IDH1* mutation status were obtained from Ceccarelli and colleagues' study[65]. The content of immune cells was computed with xCell pre-calculated scores downloaded from the xCell website[45]. The genes encoding MHCII and CD74 proteins were selected based on the literature[24,66,67]. The expression profiles were clustered using hierarchical clustering. Significance of the clustering was computed using Fisher's exact test. Separation

566 of glioma samples was done for each grade separately. Neither WHO grade IV nor grade III
567 glioma samples were significantly discriminated by the expression levels of the selected
568 genes (data not shown).
569
570 **Immunohistochemistry on brain slices**
571 For tissue collection for histology, mice were anesthetized and transcardially perfused with
572 PBS and 4% paraformaldehyde (PFA). Tissues were dissected, and the brain was post fixed
573 in 4% PFA overnight and then placed in 30% sucrose for 2 days, embedded in Tissue-Tek
574 O.C.T Compound, and 10 µm cryosections were cut and stored at -80 °C. Cryosections were
575 blocked in PBS containing 10% donkey serum in 0.1% Triton X-100 solution for 2 hours and
576 incubated overnight at 4 °C with goat anti-AIF-1/Iba1 antibody (Novus Biologicals;
577 Centennial, Colorado, USA; dilution 1:200, 3% donkey serum, 0.1% Triton X-100) and rabbit
578 anti-TMEM119 antibody (Synaptic Systems; Goettingen, Germany, dilution 1:500, 3%
579 donkey serum, 0.1% Triton X-100). Next, sections were washed in PBS, incubated with a
580 donkey anti-goat Alexa Fluor 647 and donkey anti-rabbit Alexa Fluor 488 (Invitrogen;
581 Waltham, Massachusetts, USA; dilution 1:1000, 3% donkey serum, 0.1% Triton X-100) for 2
582 hours at room temperature. Nuclei were counter-stained with DAPI (0.1mg/mL), and images
583 were obtained using a Leica DM8000 fluorescent microscope.
584
585 **Data availability**

586 Bam files and Seurat v3 processed gene expression matrix for each condition can be
587 downloaded from the NIH GEO database (TBD).
588
589
590
591
592
593 **References**

594 1. Binnewies, M. et al. Understanding the tumor immune microenvironment (TIME) for
595 effective therapy. Nat. Med. (2018). doi:10.1038/s41591-018-0014-x

596 2. Qian, B.-Z. & Pollard, J. W. Macrophage diversity enhances tumor progression and
597 metastasis. Cell (2010). doi:10.1016/j.cell.2010.03.014

598 3. Walentynowicz, K. A. et al. In search for reliable markers of glioma-induced
599 polarization of microglia. Front. Immunol. (2018). doi:10.3389/fimmu.2018.01329

600 4. Szulzewsky, F. *et al.* Glioma-associated microglia/macrophages display an expression
601 profile different from M1 and M2 polarization and highly express Gpnmb and Spp1.
602 *PLoS One* **10**, (2015).

603 5. Szulzewsky, F. *et al.* Human glioblastoma-associated microglia/monocytes express a
604 distinct RNA profile compared to human control and murine samples. *Glia* **64**, 1416–
605 1436 (2016).

606 6. Gieryng, A. *et al.* Immune microenvironment of experimental rat C6 gliomas resembles
607 human glioblastomas. *Sci. Rep.* (2017). doi:10.1038/s41598-017-17752-w

608 7. Bowman, R. L. *et al.* Macrophage Ontogeny Underlies Differences in Tumor-Specific
609 Education in Brain Malignancies. *Cell Rep.* **17**, 2445–2459 (2016).

610 8. Müller, S. *et al.* Single-cell profiling of human gliomas reveals macrophage ontogeny
611 as a basis for regional differences in macrophage activation in the tumor
612 microenvironment. *Genome Biol.* (2017). doi:10.1186/s13059-017-1362-4

613 9. Darmanis, S. *et al.* Single-Cell RNA-Seq Analysis of Infiltrating Neoplastic Cells at the
614 Migrating Front of Human Glioblastoma. *Cell Rep.* (2017).
615 doi:10.1016/j.celrep.2017.10.030

616 10. Venteicher, A. S. *et al.* Decoupling genetics, lineages, and microenvironment in IDH-
617 mutant gliomas by single-cell RNA-seq. *Science (80-.).* **355**, eaai8478 (2017).

618 11. Yang, W. *et al.* Sex differences in GBM revealed by analysis of patient imaging,
619 transcriptome, and survival data. *Sci. Transl. Med.* (2019).
620 doi:10.1126/scitranslmed.aao5253

621 12. Conforti, F. *et al.* Cancer immunotherapy efficacy and patients' sex: a systematic
622 review and meta-analysis. *Lancet Oncol.* (2018). doi:10.1016/S1470-2045(18)30261-4

623 13. Guneykaya, D. *et al.* Transcriptional and Translational Differences of Microglia from
624 Male and Female Brains. *Cell Rep.* (2018). doi:10.1016/j.celrep.2018.08.001

625 14. Villa, A. *et al.* Sex-Specific Features of Microglia from Adult Mice. *Cell Rep.* (2018).
626 doi:10.1016/j.celrep.2018.05.048

627 15. Oh, T. *et al.* Immunocompetent murine models for the study of glioblastoma
628 immunotherapy. *Journal of Translational Medicine* (2014). doi:10.1186/1479-5876-12-
629 107

630 16. Gabrusiewicz, K. *et al.* Characteristics of the alternative phenotype of
631 microglia/macrophages and its modulation in experimental gliomas. *PLoS One* **6**,

632 (2011).

633 17. Haage, V. *et al.* Comprehensive gene expression meta-analysis identifies signature
634 genes that distinguish microglia from peripheral monocytes/macrophages in health
635 and glioma. *Acta Neuropathol. Commun.* 1–18 (2019). doi:10.1186/s40478-019-0665-
636 y

637 18. Bennett, M. L. *et al.* New tools for studying microglia in the mouse and human CNS.
638 *Proc. Natl. Acad. Sci.* (2016). doi:10.1073/pnas.1525528113

639 19. Masuda, T. *et al.* Spatial and temporal heterogeneity of mouse and human microglia at
640 single-cell resolution. *Nature* **566**, 388–392 (2019).

641 20. Matcovitch-Natan, O. *et al.* Microglia development follows a stepwise program to
642 regulate brain homeostasis. *Science (80-.).* (2016). doi:10.1126/science.aad8670

643 21. Keren-Shaul, H. *et al.* A Unique Microglia Type Associated with Restricting
644 Development of Alzheimer's Disease. *Cell* **169**, 1276-1290.e17 (2017).

645 22. Sousa, C., Biber, K. & Michelucci, A. Cellular and Molecular Characterization of
646 Microglia: A Unique Immune Cell Population. *Front. Immunol.* **8**, 198 (2017).

647 23. Kim, W.-K. *et al.* CD163 identifies perivascular macrophages in normal and viral
648 encephalitic brains and potential precursors to perivascular macrophages in blood.
649 *Am. J. Pathol.* **168**, 822–34 (2006).

650 24. Janeway, C. *Immunobiology 5 : the immune system in health and disease*. (Garland
651 Pub, 2001).

652 25. Jordão, M. J. C. *et al.* Single-cell profiling identifies myeloid cell subsets with distinct
653 fates during neuroinflammation. *Science (80-.).* **363**, eaat7554 (2019).

654 26. Goldmann, T. *et al.* Origin, fate and dynamics of macrophages at central nervous
655 system interfaces. *Nat. Immunol.* **17**, 797–805 (2016).

656 27. Ziegler-Heitbrock, L. *et al.* Nomenclature of monocytes and dendritic cells in blood.
657 *Blood* **116**, e74-80 (2010).

658 28. Thomas, G. D. *et al.* Human Blood Monocyte Subsets: A New Gating Strategy Defined
659 Using Cell Surface Markers Identified by Mass Cytometry. *Arterioscler. Thromb. Vasc.*
660 *Biol.* **37**, 1548–1558 (2017).

661 29. Fleming, T. J., Fleming, M. L. & Malek, T. R. Selective expression of Ly-6G on myeloid
662 lineage cells in mouse bone marrow. RB6-8C5 mAb to granulocyte-differentiation

663 antigen (Gr-1) detects members of the Ly-6 family. *J. Immunol.* **151**, 2399–408 (1993).

664 30. McFarland, H. I., Nahill, S. R., Maciaszek, J. W. & Welsh, R. M. CD11b (Mac-1): a
665 marker for CD8+ cytotoxic T cell activation and memory in virus infection. *J. Immunol.*
666 (1992).

667 31. Kawai, K. *et al.* CD11b-mediated migratory property of peripheral blood B cells. *J.*
668 *Allergy Clin. Immunol.* (2005). doi:10.1016/j.jaci.2005.03.021

669 32. Hickman, S. E. *et al.* The microglial sensome revealed by direct RNA sequencing. *Nat.*
670 *Neurosci.* (2013). doi:10.1038/nn.3554

671 33. Van Hove, H. *et al.* A single-cell atlas of mouse brain macrophages reveals unique
672 transcriptional identities shaped by ontogeny and tissue environment. *Nat. Neurosci.*
673 (2019). doi:10.1038/s41593-019-0393-4

674 34. Rapp, M. *et al.* CCL22 controls immunity by promoting regulatory T cell
675 communication with dendritic cells in lymph nodes. *J. Exp. Med.* (2019).
676 doi:10.1084/jem.20170277

677 35. Zumwalt, T. J., Arnold, M., Goel, A. & Boland, C. R. Active secretion of CXCL10 and
678 CCL5 from colorectal cancer microenvironments associates with GranzymeB+ CD8+
679 T-cell infiltration. *Oncotarget* (2015). doi:10.18632/oncotarget.3205

680 36. Ma, F., Zhang, C., Prasad, K. V. S., Freeman, G. J. & Schlossman, S. F. Molecular
681 cloning of Porimin, a novel cell surface receptor mediating oncotic cell death. *Proc.*
682 *Natl. Acad. Sci.* (2001). doi:10.1073/pnas.171322898

683 37. Takekoshi, T. *et al.* Identification of a novel marker for dendritic cell maturation, mouse
684 transmembrane protein 123. *J. Biol. Chem.* (2010). doi:10.1074/jbc.M110.118877

685 38. Chen, Z. *et al.* Cellular and molecular identity of tumor-associated macrophages in
686 glioblastoma. *Cancer Res.* (2017). doi:10.1158/0008-5472.CAN-16-2310

687 39. Zhao, Y. *et al.* The immunological function of CD52 and its targeting in organ
688 transplantation. *Inflammation Research* (2017). doi:10.1007/s00011-017-1032-8

689 40. Przanowski, P., Loska, S., Cysewski, D., Dabrowski, M. & Kaminska, B. ISG'ylation
690 increases stability of numerous proteins including Stat1, which prevents premature
691 termination of immune response in LPS-stimulated microglia. *Neurochem. Int.* (2018).
692 doi:10.1016/j.neuint.2017.07.013

693 41. Goldmann, T. *et al.* USP18 lack in microglia causes destructive interferonopathy of the
694 mouse brain. *EMBO J.* (2015). doi:10.15252/embj.201490791

695 42. Tian, M. *et al.* Impact of gender on the survival of patients with glioblastoma. *Biosci.*
696 *Rep.* **0**, 1–9 (2018).

697 43. Calandra, T. & Roger, T. Macrophage migration inhibitory factor: A regulator of innate
698 immunity. *Nature Reviews Immunology* (2003). doi:10.1038/nri1200

699 44. Fan, H. *et al.* Macrophage Migration Inhibitory Factor and CD74 Regulate Macrophage
700 Chemotactic Responses via MAPK and Rho GTPase. *J. Immunol.* (2011).
701 doi:10.4049/jimmunol.1003713

702 45. Aran, D., Hu, Z. & Butte, A. J. xCell: digitally portraying the tissue cellular
703 heterogeneity landscape. *Genome Biol.* **18**, 220 (2017).

704 46. Mieczkowski, J. *et al.* Down-regulation of IKKβ expression in glioma-infiltrating
705 microglia/macrophages is associated with defective inflammatory/immune gene
706 responses in glioblastoma. *Oncotarget* **6**, 33077–90 (2015).

707 47. Müller, A., Brandenburg, S., Turkowski, K., Müller, S. & Vajkoczy, P. Resident
708 microglia, and not peripheral macrophages, are the main source of brain tumor
709 mononuclear cells. *Int. J. Cancer* (2015). doi:10.1002/ijc.29379

710 48. Chen, Z., Ross, J. L. & Hambardzumyan, D. Intravital 2-photon imaging reveals
711 distinct morphology and infiltrative properties of glioblastoma-associated
712 macrophages. *Proc. Natl. Acad. Sci.* (2019). doi:10.1073/pnas.1902366116

713 49. Gosselin, D. *et al.* An environment-dependent transcriptional network specifies human
714 microglia identity. *Science (80-.).* **356**, eaal3222 (2017).

715 50. Lavin, Y. *et al.* Tissue-resident macrophage enhancer landscapes are shaped by the
716 local microenvironment. *Cell* **159**, 1312–1326 (2014).

717 51. Griffith, J. W., Sokol, C. L. & Luster, A. D. Chemokines and chemokine receptors:
718 positioning cells for host defense and immunity. *Annu. Rev. Immunol.* **32**, 659–702
719 (2014).

720 52. Mu, L. *et al.* CD4+ and Perivascular Foxp3+ T Cells in Glioma Correlate with
721 Angiogenesis and Tumor Progression. *Front. Immunol.* **8**, 1451 (2017).

722 53. Han, S. *et al.* Tumour-infiltrating CD4(+) and CD8(+) lymphocytes as predictors of
723 clinical outcome in glioma. *Br. J. Cancer* **110**, 2560–8 (2014).

724 54. Cook, M. B., McGlynn, K. A., Devesa, S. S., Freedman, N. D. & Anderson, W. F. Sex
725 disparities in cancer mortality and survival. *Cancer Epidemiol. Biomarkers Prev.*
726 (2011). doi:10.1158/1055-9965.EPI-11-0246

727 55. Vegeto, E. *et al.* Estrogen Prevents the Lipopolysaccharide-Induced Inflammatory
728 Response in Microglia. *J. Neurosci.* (2018). doi:10.1523/jneurosci.21-06-01809.2001

729 56. Golomb, M. R., Fullerton, H. J., Nowak-Gottl, U. & Deveber, G. Male predominance in
730 childhood ischemic stroke: Findings from the international pediatric stroke study.
731 *Stroke* (2009). doi:10.1161/STROKEAHA.108.521203

732 57. Spychala, M. S., Honarpisheh, P. & McCullough, L. D. Sex differences in
733 neuroinflammation and neuroprotection in ischemic stroke. *Journal of Neuroscience*
734 *Research* (2017). doi:10.1002/jnr.23962

735 58. Zheng, G. X. Y. *et al.* Massively parallel digital transcriptional profiling of single cells.
736 *Nat. Commun.* (2017). doi:10.1038/ncomms14049

737 59. Stuart, T. *et al.* Comprehensive Integration of Single-Cell Data. *Cell* **177**, 1888-
738 1902.e21 (2019).

739 60. Butler, A., Hoffman, P., Smibert, P., Papalexi, E. & Satija, R. Integrating single-cell
740 transcriptomic data across different conditions, technologies, and species. *Nat.*
741 *Biotechnol.* **36**, 411–420 (2018).

742 61. Tirosh, I. *et al.* Dissecting the multicellular ecosystem of metastatic melanoma by
743 single-cell RNA-seq. *Science* **352**, 189–96 (2016).

744 62. Maaten, L. van der & Hinton, G. Visualizing Data using t-SNE. *J. Mach. Learn. Res.* **9**,
745 2579–2605 (2008).

746 63. McInnes, L., Healy, J., Saul, N. & Großberger, L. UMAP: Uniform Manifold
747 Approximation and Projection. *J. Open Source Softw.* (2018). doi:10.21105/joss.00861

748 64. Yu, G., Wang, L.-G., Han, Y. & He, Q.-Y. clusterProfiler: an R Package for Comparing
749 Biological Themes Among Gene Clusters. *Omi. A J. Integr. Biol.* (2012).
750 doi:10.1089/omi.2011.0118

751 65. Ceccarelli, M. *et al.* Molecular Profiling Reveals Biologically Discrete Subsets and
752 Pathways of Progression in Diffuse Glioma. *Cell* **164**, 550–563 (2016).

753 66. van Lith, M., McEwen-Smith, R. M. & Benham, A. M. HLA-DP, HLA-DQ, and HLA-DR
754 have different requirements for invariant chain and HLA-DM. *J. Biol. Chem.* **285**,
755 40800–8 (2010).

756 67. Lefranc, M.-P. *et al.* IMGT®, the international ImMunoGeneTics information system®
757 25 years on. *Nucleic Acids Res.* **43**, D413–D422 (2015).

Figure legends

Fig. 1. Identification of immune cell populations in control and tumor-bearing brain hemispheres. a Scheme of the experimental workflow. **b** t-SNE plot demonstrating clustering obtained for each group (female control, female tumor, male control, male tumor), 2 biological replicates were combined. Clusters annotations: MG – microglia, pre-MG – premature microglia, Mo – Monocytes, intMoMΦ – intermediate Monocyte-Macrophage, MΦ – macrophages, BAM – CNS border-associated macrophages, DCs – dendritic cells, Ncam1+- Ncam1 positive cells, NK – natural killer cells, NKT – natural killer T cells, B cells – B lymphocytes, T cells – T lymphocytes. **c** Expression of "signature" genes selected from the immune marker panel for identification of a cluster cell type (Suppl. Table 1). **d** Pie charts demonstrating distribution of the identified cell types across samples.

Fig. 2. Transcriptomic characterization of main myeloid subpopulations. a Projection of cells combined from clusters identified as microglia, monocytes/macrophages (Mo/MΦ), and BAMs from all groups. **b** Top 10 differentially expressed genes for the three main identified cell populations. **c-g** Expression level of novel and previously identified "signature" genes for microglia (**c**), macrophages (**d**), microglia and macrophages in gliomas (**e**), and BAMs (**f**). **g** Feature plots depict distribution of the expression of genes discriminating monocytes/macrophages (Mo/MΦ), Monocytes (Mo), Monocyte-Macrophage intermediate (intMoMΦ), and Macrophage (MΦ) subpopulations. **h** Density plots demonstrate the expression level of markers discriminating Mo/MΦ subpopulations. **i** UMAP plot shows clusters of Mo/MΦ subpopulations.

Fig. 3. Tumor-derived microglia and macrophages form separate cell populations. a A UMAP plot demonstrates the distribution of CD11b+ cells from naïve and tumor-bearing mice. **b** Distribution of microglia and Mo/MΦ "signature" gene scores (presented as an average of expression of the selected genes). **c** Density plots of microglia and Mo/MΦ scores across MG and Mo/MΦ populations demonstrating no overlap of a specific "signature" between the two cell populations. **d** Cell hierarchical clustering according to the expression of reported macrophage markers demonstrates bimodal cell distribution. **e, f** Immunohistochemical staining for microglia (Iba+, Tmem119+) and Mo/MΦ (Iba+, Tmem119-) shows the localization of specific immune cells within the tumor and its surroundings in male (**e**) and female (**f**) animals; a dashed line marks the tumor edge; scale – 100 μm.

Fig. 4. Functional analysis of glioma-activated microglia in comparison to tumor-infiltrating monocytes/macrophages. a–b Heatmaps show significantly upregulated genes in homeostatic microglia (Hom-MG) vs activated microglia (Act-MG) **(a)** and Act-MG vs Mo/MΦ **(b**). Differentially upregulated genes in those cells have been tested further. **c** Scatter

plot depicts levels of differentially upregulated genes in Act-MG and Mo/MΦ. **d** Heatmap shows the comparison of expression of top 25 upregulated genes in Act-MG and Mo/MΦ. Gene Ontology analysis of biological processes for genes upregulated in (**e**) Act-MG compared to Hom-MG and (**f**) for genes upregulated in Mo/MΦ compared to the Act-MG. **g-h** Expression levels of selected genes expressed specifically in distinct subpopulations

Fig. 5. Expression *of MHC II* and *Cd74* genes is more abundant in microglia and monocytes/macrophages from gliomas in males. a UMAP plots demonstrate the distribution of male and female cells across cell clusters and reveals sex-enriched areas. **b** Volcano plots depict differentially expressed genes across sexes in Act-MG and Mo/MΦ infiltrating gliomas. **c** Expression of the most highly upregulated genes from males. **d** Density plots show enrichment of male cells in *MHCII*- and *Cd74*-high expressing gene populations of Act-MG and intMoMΦ. **e** Violin and density plots demonstrate that *Mif* upregulation is limited to the intMoMΦ *MHCII*^{high} cells. **h** Flow cytometry analysis shows the increased infiltration of CD4+ cells to male TME compared with female TME. **g** Normalized log2 RNA-seq counts for *MHCII* complex genes from TCGA WHO grade II glioma patients' data set show significant differences between male and female glioma patients (Fisher's exact test).

Figure 1

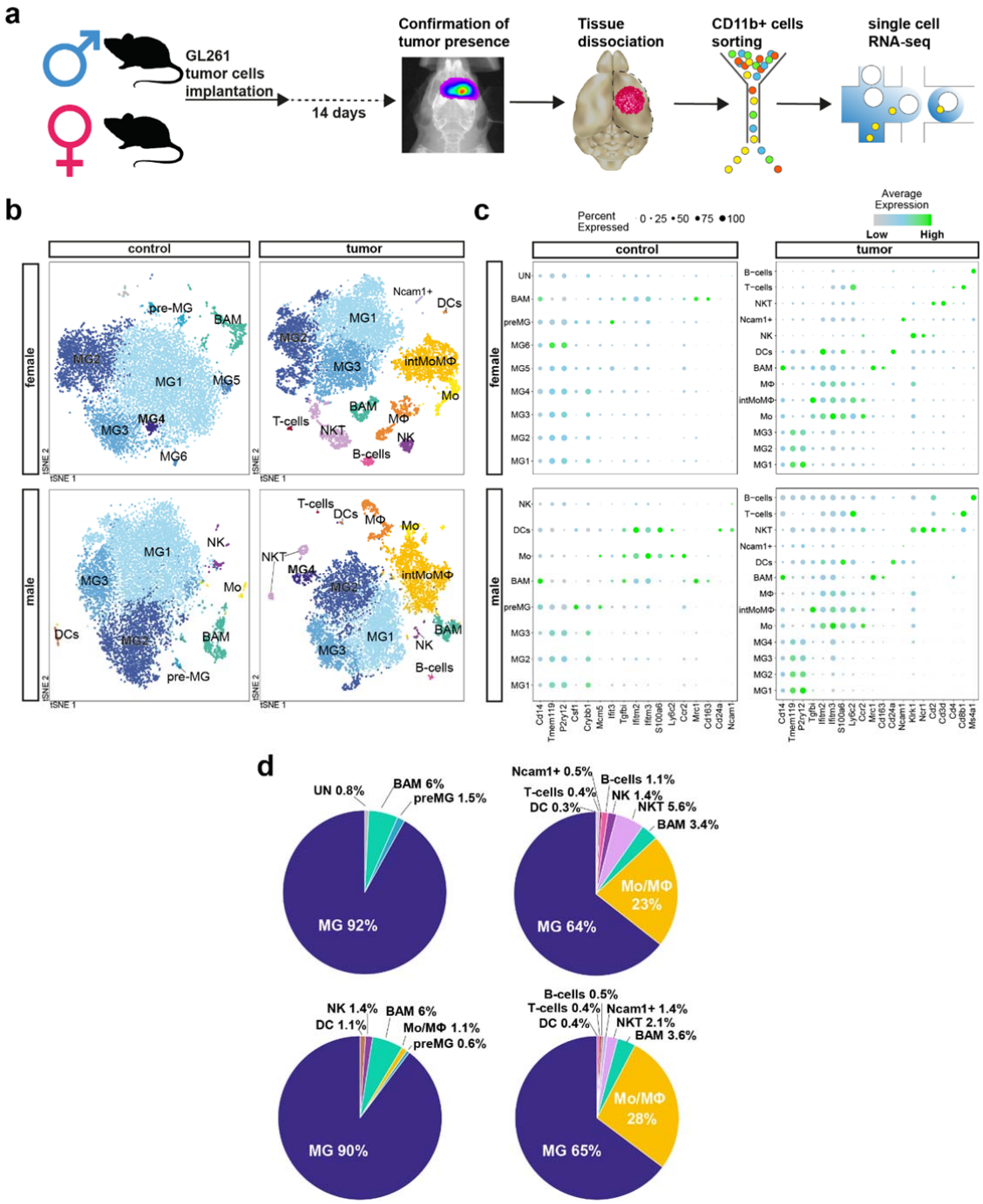
a
GL261
tumor cells
implantation
14 days
Confirmation of
tumor presence
Tissue
dissociation
CD11b+ cells
sorting
single cell
RNA-seq
b
control
tumor
female
male
pre-MG
BAM
MG2
MG1
MG5
MG4
MG3
MG6
Ncam1+
DCs
intMoMΦ
Mo
T-cells
NKT
MΦ
NK
B-cells
tSNE 1
tSNE 2
c
Percent
Expressed
0 25 50 75 100
Average
Expression
Low
High
UN
BAM
preMG
MG6
MG5
MG4
MG3
MG2
MG1
B−cells
T−cells
NKT
Ncam1+
NK
DCs
MΦ
intMoMΦ
Mo
Cd14
Tmem119
P2ry12
Csf1
Crybb1
Mcm5
Ifit3
Tgfbi
Ifitm2
Ifitm3
S100a6
Ly6c2
Ccr2
Mrc1
Cd163
Cd24a
Ncam1
Nkx1
Nkx1
Cd2
Cd3d
Cd4
Cd8b1
Ms4a1
d
UN 0.8%
BAM 6%
preMG 1.5%
MG 92%
Ncam1+ 0.5%
T-cells 0.4%
DC 0.3%
B-cells 1.1%
NK 1.4%
NKT 5.6%
BAM 3.4%
Mo/MΦ
23%
MG 64%
NK 1.4%
DC 1.1%
BAM 6%
Mo/MΦ 1.1%
preMG 0.6%
MG 90%
B-cells 0.5%
T-cells 0.4%
DC 0.4%
Ncam1+ 1.4%
NKT 2.1%
BAM 3.6%
Mo/MΦ
28%
MG 65%

Figure 2

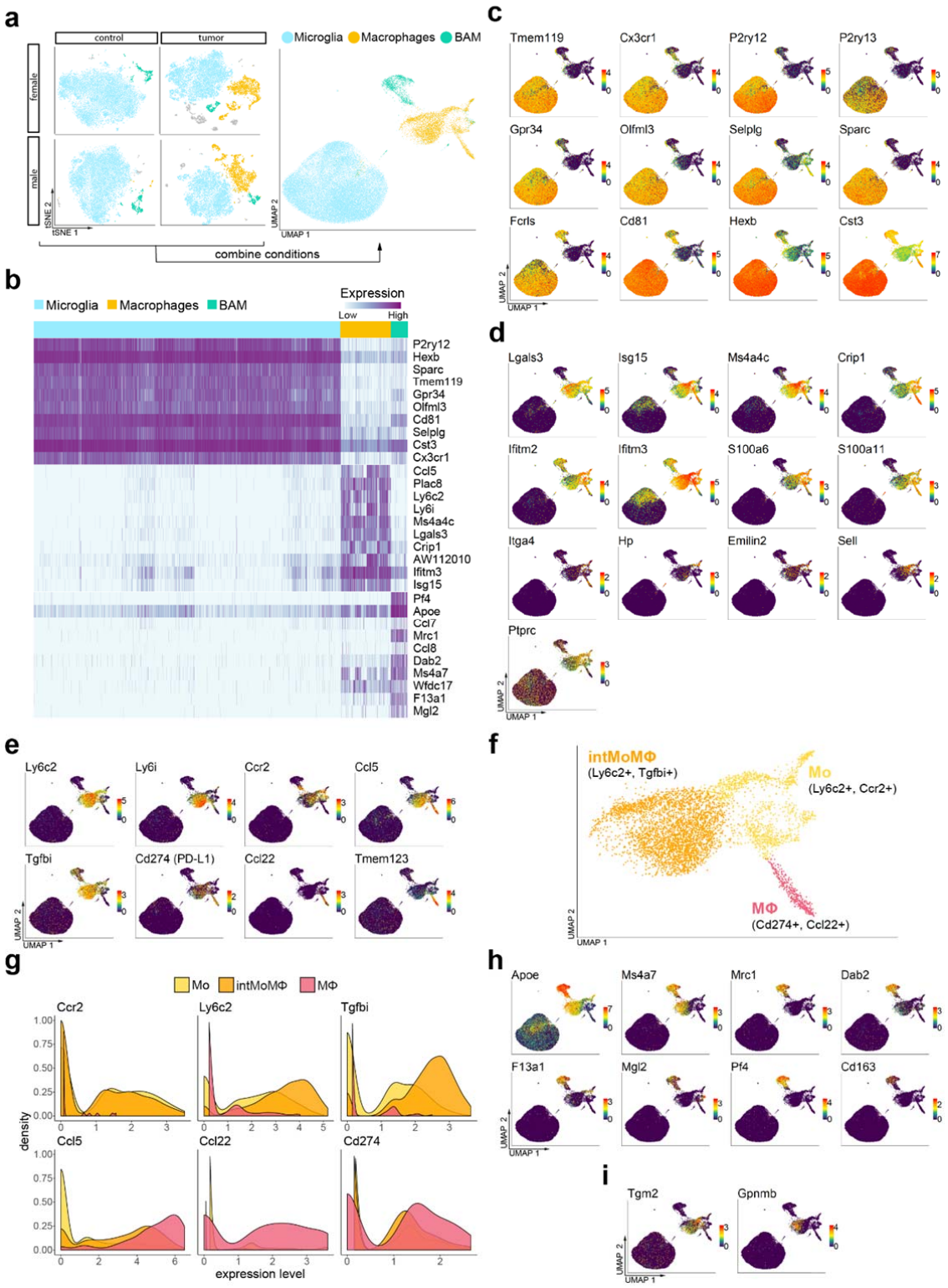

815

816

Figure 3

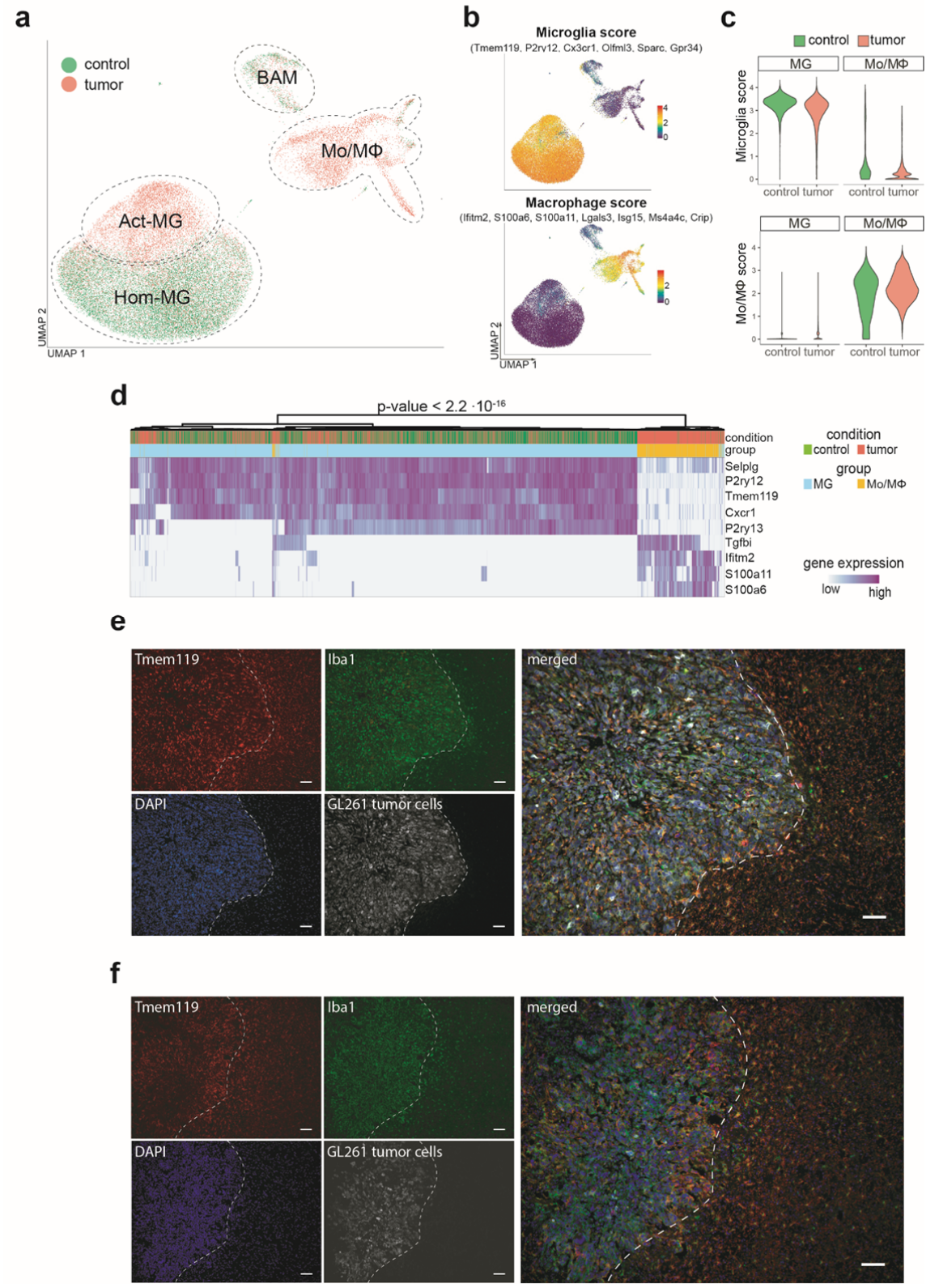
a
control
tumor
BAM
Mo/MΦ
Act-MG
Hom-MG
UMAP 2
UMAP 1
b
Microglia score
(Tmem119, P2ry12, Cx3cr1, Olfml3, Sparc, Gpr34)
Macrophage score
(Ifitm2, S100a6, S100a11, Lgals3, Isg15, Ms4a4c, Crip)
c
control
tumor
MG
Mo/MΦ
Microglia score
Mo/MΦ score
control tumor
d
p-value < 2.2 ·10-16
condition
group
Selplg
P2ry12
Tmem119
Cxcr1
P2ry13
Tgfbi
Ifitm2
S100a11
S100a6
condition
control
tumor
group
MG
Mo/MΦ
gene expression
low
high
e
Tmem119
Iba1
merged
DAPI
GL261 tumor cells
f
Tmem119
Iba1
merged
DAPI
GL261 tumor cells

817

Figure 4

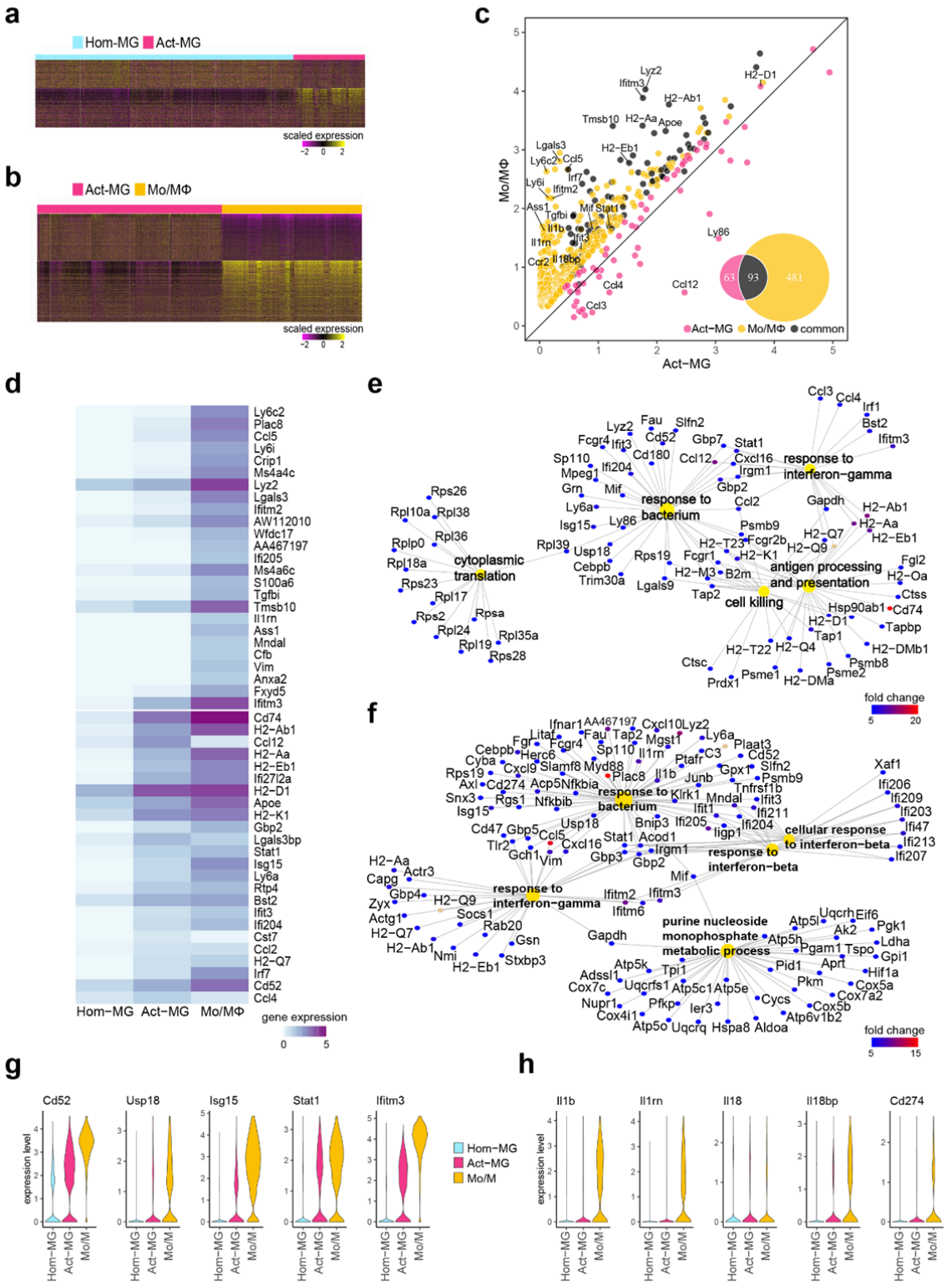
a
Hom-MG Act-MG
scaled expression
b
Act-MG Mo/MΦ
scaled expression
c
Mo/MΦ
Act-MG
Act-MG Mo/MΦ common
63 93 481
d
Hom-MG Act-MG Mo/MΦ
gene expression
e
response to interferon-gamma
response to bacterium
cytoplasmic translation
antigen processing and presentation
cell killing
fold change
f
response to bacterium
response to interferon-gamma
response to interferon-beta
cellular response to interferon-beta
purine nucleoside monophosphate metabolic process
fold change
g
Cd52
Usp18
Isg15
Stat1
Ifitm3
expression level
Hom-MG
Act-MG
Mo/M
h
Il1b
Il1rn
Il18
Il18bp
Cd274
expression level

818

Figure 5

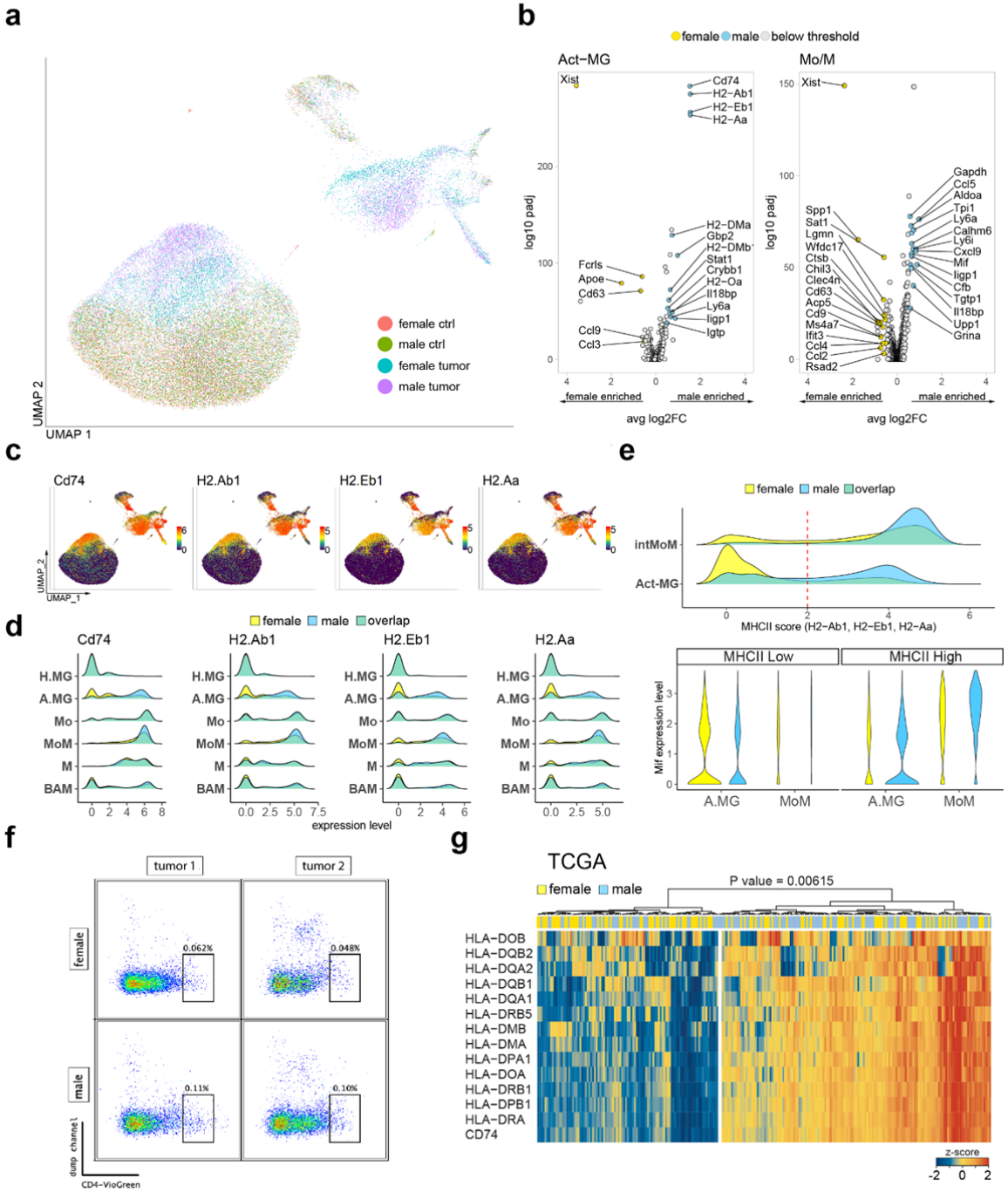
a
UMAP 2
UMAP 1
female ctrl
male ctrl
female tumor
male tumor
b
female male below threshold
Act−MG
Mo/M
Xist
Cd74
H2−Ab1
H2−Eb1
H2−Aa
H2−DMa
Gbp2
H2−DMb
Stat1
Crybb1
H2−Oa
Il18bp
Ly6a
Iigp1
Igtp
Fcrls
Apoe
Cd63
Ccl9
Ccl3
Gapdh
Ccl5
Aldoa
Tpi1
Ly6a
Calhm6
Ly6i
Cxcl9
Mif
Iigp1
Cfb
Tgtp1
Il18bp
Upp1
Grina
Spp1
Sat1
Lgmn
Wfdc17
Ctsb
Chil3
Clec4n
Cd63
Acp5
Cd9
Ms4a7
Ifit3
Ccl4
Ccl2
Rsad2
log10 padj
female enriched
male enriched
avg log2FC
c
Cd74
H2.Ab1
H2.Eb1
H2.Aa
UMAP_2
UMAP_1
d
female male overlap
H.MG
A.MG
Mo
MoM
M
BAM
expression level
e
female male overlap
intMoM
Act-MG
MHCII score (H2−Ab1, H2−Eb1, H2−Aa)
MHCII Low
MHCII High
Mif expression level
A.MG
MoM
f
tumor 1
tumor 2
female
male
0.062%
0.048%
0.11%
0.10%
dump channel
CD4−VioGreen
g
TCGA
female male
P value = 0.00615
HLA−DOB
HLA−DQB2
HLA−DQA2
HLA−DQB1
HLA−DQA1
HLA−DRB5
HLA−DMB
HLA−DMA
HLA−DPA1
HLA−DOA
HLA−DRB1
HLA−DPB1
HLA−DRA
CD74
z-score

819